



VOC oxidation over $\text{MnO}_x\text{--CeO}_2$ catalysts prepared by a combustion method

Dimitrios Delimaris^{a,b}, Theophilos Ioannides^{a,*}

^a Foundation for Research and Technology-Hellas, Institute of Chemical Engineering and High Temperature Chemical Processes (FORTH/ICE-HT), P.O. Box 1414, GR-26504 Patras, Greece

^b Department of Chemistry, University of Patras, GR-26504 Patras, Greece

ARTICLE INFO

Article history:

Received 11 February 2008

Received in revised form 3 April 2008

Accepted 5 April 2008

Available online 11 April 2008

Keywords:

VOC

Oxidation

Ethanol

Ethyl acetate

Toluene

Ceria

Manganese oxide

Compensation effect

ABSTRACT

$\text{MnO}_x\text{--CeO}_2$ catalysts were prepared by a urea combustion method and their performance in the oxidation of ethanol, ethyl acetate and toluene was evaluated. XRD, XPS, H_2 -TPR and N_2 physisorption were employed in catalyst characterization. Mn^{2+} and Mn^{3+} ions are present in the catalysts. In ceria-rich materials, crystalline manganese oxide phases are absent and Mn ions are homogeneously distributed between the bulk and the surface suggesting incorporation of Mn ions in ceria structure. In Mn-rich materials, segregation of a Mn_3O_4 phase takes place. The mixed oxides get reduced by H_2 at lower temperatures than the corresponding single oxides and Mn ions promote reduction of ceria. The surface area of $\text{MnO}_x\text{--CeO}_2$ catalysts is larger than the one of single oxides prepared with the same method. The larger surface area of $\text{MnO}_x\text{--CeO}_2$ catalysts counterbalances their smaller specific activity allowing complete conversion of the examined VOCs at lower temperatures compared to the single oxides.

© 2008 Elsevier B.V. All rights reserved.

1. Introduction

Volatile organic compounds (VOC) are major air pollutants, and catalytic combustion is one important technology for eliminating VOC emissions, as it takes place at temperatures lower than those required for thermal incineration. Noble metal (Pt, Pd) catalysts, supported on Al_2O_3 or other oxides [1,2] are considered as state-of-the-art catalysts in VOC combustion. Metal oxide catalysts are also studied as cheaper alternatives to noble metals. In certain cases, metal oxides can be actually more active than noble metal catalysts. Lahousse et al. [3] have showed that $\gamma\text{-MnO}_2$ is more active than Pt/TiO_2 in the oxidation of representative VOCs.

Manganese oxides are among the most active oxide catalysts in VOC oxidation [3–7]. The $\gamma\text{-MnO}_2$ phase has been reported to be more active than $\beta\text{-MnO}_2$ or Mn_2O_3 in the oxidation of ethanol [5–7]. The cryptomelane-type manganese OMS-2 has been also studied in the oxidation of ethyl acetate [8]. MnO_x catalysts supported on Al_2O_3 , TiO_2 and $\text{ZrO}_2(\text{Y}_2\text{O}_3)$ have been studied in ethanol and ethyl acetate oxidation [9,10], while the oxidation of toluene over Mg/Mn/Al catalysts prepared by LDH precursors has been investigated by Dula et al. [11]. The Mn–Ce–O catalytic

system has been the subject of a number of studies due to the favourable properties of ceria in oxidation catalysis. Thus, $\text{MnO}_x\text{--CeO}_2$ catalysts have been examined in the oxidation of ethanol [12], formaldehyde [13] and hexane [14], in the wet oxidation of phenol [15] and acrylic acid [16], as well as in the SCR of NO with NH_3 [17] and in catalytic NO_x sorption [18]. $\text{MnO}_x\text{--CeO}_2$ catalysts were prepared by co-precipitation methods in Refs. [13–18]. Sol-gel methods, employing citric acid, were applied in Refs. [12,13].

We have previously reported on the application of the combustion method, as a fast and simple technique for synthesis of mixed oxide catalysts, such as CuO--CeO_2 [19] and CuO--MnO_x [20], with favourable catalytic performance. In the present work, $\text{MnO}_x\text{--CeO}_2$ catalysts spanning the whole composition range have been prepared via the combustion method and their catalytic properties in the oxidation of ethanol, ethyl acetate and toluene have been evaluated. Catalysts were characterized by XRD, XPS, H_2 -TPR and N_2 physisorption with the aim to assess possible synergy effects on catalytic performance.

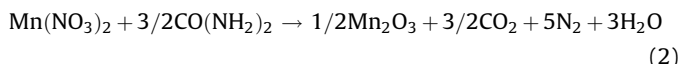
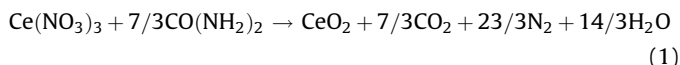
2. Experimental

2.1. Catalyst preparation

$\text{MnO}_x\text{--CeO}_2$ catalysts were prepared via the urea–nitrate combustion method using urea and nitrate salts as starting

* Corresponding author. Tel.: +30 2610 965264; fax: +30 2610 965223.
E-mail address: theo@iceht.forth.gr (T. Ioannides).

compounds. The combustion of urea with manganese and cerium nitrate salts can be written as follows:



According to the above reactions, the stoichiometric ratios of urea to the metal salt are 2.33 for cerium and 1.5 for manganese. For a mixed Mn–Ce oxide, the stoichiometric ratio takes values in the range 1.5–2.33 depending on the final composition. In the present work, the amount of urea used in catalyst preparation was higher than stoichiometry with equivalence ratio, Φ (Φ = actual urea/stoichiometric urea) in the range of 1.5–7.3.

Nitrate salts of manganese and cerium with the selected molar ratio were mixed with appropriate amounts of urea and the mixture was preheated to 80 °C to remove excess water. The resulting viscous gel was placed in a tubular furnace kept inside a fume hood and maintained at 500 °C. After a short period, ignition took place with rapid evolution of a large quantity of gases, yielding a voluminous powder. The powder was further calcined at 550 °C for 2 h in order to remove any remaining carbon residues. 0.5 g of catalyst was produced in each preparation. Keeping the amount of produced catalyst constant ensures the repeatability of the process. Parameters of synthesis were the Mn/(Mn + Ce) atomic ratio and the equivalence ratio, Φ . Catalysts are coded as $\text{Mn}_x\text{Ce}_{1-x}$, where x is the Mn/(Mn + Ce) atomic ratio. Catalysts with $x = 0, 0.05, 0.15, 0.25, 0.50, 0.75$ or 1 were prepared. Commercial samples of MnO_2 , Mn_2O_3 and Mn_3O_4 , Aldrich, were also examined for comparison purposes.

2.2. Catalyst characterization

The surface area and pore size distribution of the samples were determined from the isotherms of nitrogen physisorption at liquid nitrogen temperature in an automated apparatus (Autosorb-1, Quantachrome Corporation). Prior to measurement, the samples were outgassed at 150 °C for 2 h. The surface area was calculated via the BET equation, while the BJH method was employed for calculating the pore size distribution from the desorption branch of the isotherms.

The crystalline structure of the catalysts was analyzed by means of an X-ray powder diffractometer (D8 Advance Bruker AXS) employing Cu K α radiation ($\lambda = 0.15418$ nm) and a Lynx Eye Position Sensitive Detector. The scan speed during analysis was 2 s/step.

Temperature-programmed reduction (TPR) experiments were performed under a flow of a 3% H_2/He mixture ($50 \text{ cm}^3 \text{ min}^{-1}$) with a heating rate of $10^\circ \text{C min}^{-1}$. Prior to TPR, the catalysts were treated under a 20% O_2/He mixture at 400 °C for 15 min. A mass spectrometer (Omnistar/Pfeiffer Vacuum) was used for on-line monitoring of TPR effluent gas. The sample weight was in the range of 17–265 mg depending on the manganese content of the catalysts. The above weight range was chosen based on the methodology developed in Refs. [21,22] for optimal selection of experimental parameters in a TPR experiment.

XPS measurements were done in an Ultra High Vacuum (UHV) chamber with base pressure $P < 5 \times 10^{-10}$ mbar, equipped with a SPECS LHS-10 hemispherical analyzer. The unmonochromatized Al K α line (1486.6 eV) and a constant analyzer pass energy $E_p = 97$ eV were used in all measurements. The binding energies were calculated with reference to the energy of C 1s peak of contaminant carbon at 284.6 eV. The XPS core level spectra were analyzed in

mixed Gaussian–Lorentzian peaks, using a Shirley background subtraction.

2.3. Catalytic activity tests

Catalytic activity tests were carried out in a conventional flow reactor at atmospheric pressure and reaction temperatures in the range of 140–420 °C. Prior to all catalytic tests, the samples were heated in a flowing 20 vol.% O_2/He mixture at 300 °C for 15 min as a standard pretreatment, followed by cooling down to the reaction temperature in pure He. All runs were performed using 0.06 g of catalyst (with particle size in the region $90 < d_p < 180 \mu\text{m}$) under a reactant flow rate of $50 \text{ cm}^3 \text{ min}^{-1}$ ($W/F = 0.072 \text{ g s cm}^{-3}$). Ethanol, ethyl acetate, toluene and acetic acid were chosen as representative VOCs. Their concentration in the air feed was: 1600 ppm (ethanol), 600 ppm (toluene), 1800 ppm (ethyl acetate) and 1400 ppm (acetic acid). Product and reactant analysis was done in a gas chromatograph (Shimadzu GC-14B) equipped with TCD and FID. The conversion (X) of VOCs was calculated using the following equation:

$$X = \frac{C_{\text{in}} - C_{\text{out}}}{C_{\text{in}}} \quad (3)$$

where C_{in} and C_{out} are the feed and outlet concentration of the specific VOC, respectively. The conversion (yield) to each of the products in the case of ethanol oxidation was calculated as given below:

$$X_{\text{CO}_2} = \frac{C_{\text{CO}_2 \text{ out}}/2}{C_{\text{EtOH in}}} \quad (4)$$

$$X_{\text{acetaldehyde}} = \frac{C_{\text{acetaldehyde out}}}{C_{\text{EtOH in}}} \quad (5)$$

$$X_{\text{Ethylacetate}} = \frac{2 \times C_{\text{Ethylacetate out}}}{C_{\text{EtOH in}}} \quad (6)$$

A similar calculation was done in the case of ethyl acetate oxidation taking of course into account the different stoichiometries for each product. Regarding toluene and acetic acid oxidation, CO_2 was the single product of the reaction in both cases.

3. Results and discussion

3.1. Effect of urea equivalence ratio, Φ

In preliminary experiments, $\text{Mn}_{0.25}\text{Ce}_{0.75}$ catalysts were synthesized by varying the urea equivalence ratio, Φ . The goal of these experiments was to determine the optimal value of Φ , which leads to maximization of catalyst activity in ethanol oxidation and subsequently prepare all catalysts using the selected value of Φ . Table 1 presents the BET specific surface areas, S_{BET} , and pore volume, V_p , of $\text{Mn}_{0.25}\text{Ce}_{0.75}$ catalysts prepared with different

Table 1
Specific surface area, S_{BET} , and pore volume, V_p , of $\text{Mn}_{0.25}\text{Ce}_{0.75}$ catalysts prepared with varying urea equivalence ratios, Φ

Φ	$S_{\text{BET}} (\text{m}^2 \text{ g}^{-1})$	$V_p (\text{cm}^3 \text{ g}^{-1})$
1.53	6.3	0.05
3.06	8.3	0.04
4.16	19.5	0.09
5.20	40.2	0.15
6.11	58.5	0.21
7.34	47.4	0.17

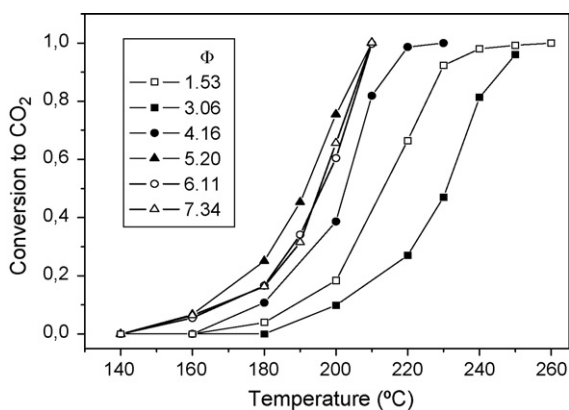


Fig. 1. Effect of equivalence ratio, Φ , employed during synthesis of $\text{Mn}_{0.25}\text{Ce}_{0.75}$ catalysts on their activity in ethanol oxidation.

equivalence ratios. Increase of Φ up to a value of 6.11 leads to increase of the specific surface area and pore volume of the catalysts. Variation of Φ leads to changes in S_{BET} by almost an order of magnitude. The beneficial effect of Φ on the surface area of the catalysts may be attributed to a “buffer” effect of excess urea, which lowers the temperature developing during autoignition of the precursor mixture and helps control the extent of sintering. The conversion to CO_2 during ethanol oxidation over $\text{Mn}_{0.25}\text{Ce}_{0.75}$ catalysts prepared with different Φ ratios is shown in Fig. 1. Although the activity trend is not monotonic with respect to specific surface area of the catalysts, the most active catalysts are those possessing the highest surface areas (Table 1) and among these the sample prepared with $\Phi = 5.20$ is the most active. Based on this result, all Mn–Ce catalysts were prepared using this value of Φ and their behaviour is presented in the following sections.

3.2. Catalyst characterization

The nitrogen adsorption/desorption isotherms of all catalysts were of type II and had type B hysteresis loops closing at $P/P_0 = 0.4$. The pore size distribution, as estimated using the BJH method, was very broad starting from 3–4 nm and extending above 100 nm indicating that the catalysts have pores in the mesopore and macropore region. The specific surface area, S_{BET} , and the pore volume, V_p , of Mn–Ce catalysts is shown in Table 2. It can be observed that the surface area (and pore volume) of pure CeO_2 and MnO_x is smaller than the one of mixed oxides. $\text{Mn}_x\text{Ce}_{1-x}$ catalysts have surface areas in the range of 38–59 $\text{m}^2 \text{g}^{-1}$ compared to values of ~ 5 and $\sim 10 \text{ m}^2 \text{g}^{-1}$ for CeO_2 and MnO_x , respectively. It appears that addition of a small amount of manganese ions to ceria

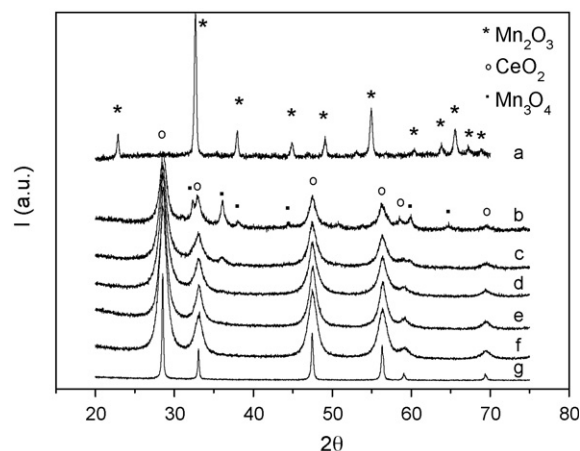


Fig. 2. XRD patterns of Mn–Ce catalysts: (a) MnO_x ; (b) $\text{Mn}_{0.75}\text{Ce}_{0.25}$; (c) $\text{Mn}_{0.5}\text{Ce}_{0.5}$; (d) $\text{Mn}_{0.25}\text{Ce}_{0.75}$; (e) $\text{Mn}_{0.15}\text{Ce}_{0.85}$; (f) $\text{Mn}_{0.05}\text{Ce}_{0.95}$; (g) CeO_2 .

or vice versa helps controlling crystallite growth during synthesis and, thus, preserve the porous structure of the materials. Similar observations have been made for Mn–Ce catalysts prepared by co-precipitation [14,15] and for Cu–Ce catalysts prepared by a modified citrate method [23].

The XRD patterns of Mn–Ce catalysts are shown in Fig. 2. In the case of pure MnO_x , all diffraction peaks can be attributed to Mn_2O_3 (JCDs 41–1442), while, in the case of pure CeO_2 all reflections are characteristic of the cubic fluorite structure (JCDs 43–1002). For Mn-rich catalysts, i.e. $\text{Mn}_{0.75}\text{Ce}_{0.25}$ and $\text{Mn}_{0.5}\text{Ce}_{0.5}$, reflections of Mn_3O_4 (hausmannite, JCDs 24–0734) are present in addition to those of ceria. On the other hand, only broad peaks of CeO_2 and no peaks of manganese oxide phases are found on catalysts with atomic ratio $\text{Mn}/(\text{Ce} + \text{Mn}) < 0.5$. The absence of manganese oxide phases in Ce-rich materials has been reported previously for catalysts prepared by co-precipitation [14,15,17,18] and combustion [24] methods and is attributed to formation of a solid solution between Mn_2O_3 and CeO_2 , as these two phases bear certain structural similarities. Replacement of Ce^{4+} by Mn^{3+} (or Mn^{2+}) in the fluorite structure should cause a decrease in its lattice constant due to the smaller size of manganese ions. As shown in Table 2, a decrease of the lattice constant of ceria was evidenced upon addition of manganese ions. Kang et al. [25] have found that the solubility limit of Mn ions in CeO_2 is 5–10 at.% after heat treatment at 1300 °C with Mn^{2+} being the incorporated ion due to its better

Table 2
Structural characteristics of Mn–Ce catalysts

Sample	S_{BET} ($\text{m}^2 \text{g}^{-1}$)	$d_{(111)}$ (nm)	V_p ($\text{cm}^3 \text{g}^{-1}$)	Lattice constant, a (nm) ^a
CeO_2	4.8	82.1	0.06	0.54187
$\text{Mn}_{0.05}\text{Ce}_{0.95}$	59.4	7.5	0.18	0.54151
$\text{Mn}_{0.15}\text{Ce}_{0.85}$	50.0	8.1	0.25	0.54106
$\text{Mn}_{0.25}\text{Ce}_{0.75}$	47.3	8.2	0.20	0.54116
$\text{Mn}_{0.5}\text{Ce}_{0.5}$	48.8	7.2	0.20	0.54186
$\text{Mn}_{0.75}\text{Ce}_{0.25}$	38.2	8.6	0.21	0.54221
MnO_x	10.3	27.6	0.11	—
Mn_2O_3^b	1.8	—	0.09	—
Mn_3O_4^b	2.0	—	0.04	—
MnO_2^b	0.6	—	0.04	—

^a Calculated from the CeO_2 (3 1 1) crystallographic plane.

^b Commercial MnO_x samples.

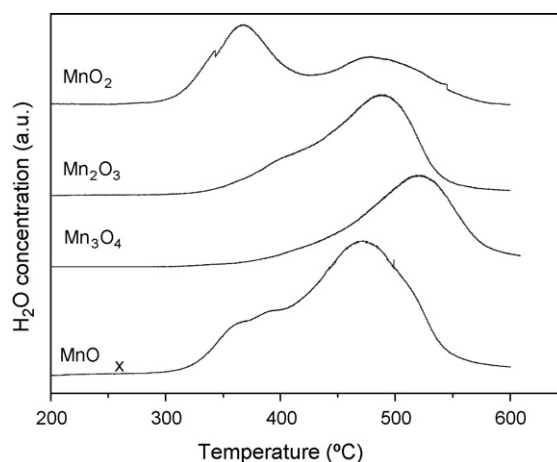


Fig. 3. TPR profiles of MnO_x and commercial Mn_3O_4 , Mn_2O_3 and MnO_2 .

Table 3
Amounts of produced water during H₂-TPR measurements

Sample	TPR (mmol H ₂ O g ⁻¹)	Mn ₃ O ₄ → MnO (mmol H ₂ O g ⁻¹)	Mn ₂ O ₃ → MnO (mmol H ₂ O g ⁻¹)	MnO ₂ → MnO (mmol H ₂ O g ⁻¹)	Reduction extent Ce ⁴⁺ → Ce ³⁺ (%)
Mn _{0.05} Ce _{0.95}	1.2	0.10	0.15	0.30	37.1 (37.9) ^a
Mn _{0.15} Ce _{0.85}	1.5	0.31	0.47	0.94	38.4 (44.4) ^a
Mn _{0.25} Ce _{0.75}	2.3	0.56	0.84	1.66	58.0 (69.1) ^a
Mn _{0.5} Ce _{0.5}	2.1	1.34	1.99	3.86	5.5 (37.8) ^a
Mn _{0.75} Ce _{0.25}	3.3	2.49	3.67	6.93	0 (65.0) ^a
MnO _x	6.5	4.37	6.33	11.5	–
Mn ₂ O ₃ ^b	5.1	–	6.33	–	–
Mn ₃ O ₄ ^b	3.7	4.37	–	–	–
MnO ₂ ^b	9.7	–	–	11.5	–

^a Values in parentheses assuming manganese as Mn₃O₄.

^b Commercial MnO_x samples.

size compatibility with Ce⁴⁺ compared to Mn³⁺. The values of the average crystallite size of CeO₂, as calculated using Scherrer's equation, are also reported in Table 2. Pure CeO₂ has a crystallite size of 82 nm, which becomes 7–8 nm for all Mn–Ce catalysts. This is in accordance with the surface area measurements, which show that CeO₂ has an order of magnitude lower surface area than Mn–Ce catalysts.

TPR profiles of commercial manganese oxides and of the pure MnO_x sample prepared by combustion are presented in Fig. 3, which depicts the water concentration in the reactor effluent as a function of temperature (the profile of water was identical to that of consumed hydrogen). Reduction of pure MnO_x takes place in the form of two overlapping peaks at 370 and 470 °C. Regarding the commercial manganese oxides, the TPR profile of MnO₂ is characterized by two peaks at 365 and 475 °C, the one of Mn₂O₃ by a peak at 490 °C with a low-temp shoulder and the one of Mn₃O₄ by a peak at 520 °C. Comparison of the shape and position of TPR profiles shows that the profile of the combustion-prepared sample is quite similar to the one of commercial Mn₂O₃. This is in agreement with the XRD data, which showed that the crystalline phase of pure MnO_x corresponds to Mn₂O₃. An additional proof of this can be derived from the amounts of water produced during TPR, which are presented in Table 3. The water produced during reduction of pure MnO_x is 6.5 mmol g⁻¹, which is very close to the theoretical value of 6.33 mmol g⁻¹ corresponding to the reduction of Mn₂O₃ to MnO. Moreover, deconvolution of the TPR profile of pure MnO_x into two peaks reveals that the amount of water in each peak is 1.76 and 4.74 mmol H₂O g⁻¹, which compares well to the theoretical amounts of water produced in the reduction steps Mn₂O₃ → Mn₃O₄ and Mn₃O₄ → MnO (1.96 and 4.37 mmol g⁻¹, respectively). Based on the above, reduction of pure MnO_x corresponds to a two-step process: The first step involves the reduction of Mn₂O₃ to Mn₃O₄, while the second step represents the reduction of Mn₃O₄ to MnO. This observation is in good agreement with previous reports [14,26].

In contrast to pure MnO_x, the reduction profiles of Mn_xCe_{1-x} catalysts are more complicated (Fig. 4). The reduction commences at lower temperatures than pure MnO_x and takes place over a rather broad temperature range (150–600 °C) with several overlapping peaks. The reduction of the Mn_{0.05}Ce_{0.95} catalyst starts at 220 °C and still continues at 600 °C, which is the final temperature of the TPR run. In the case of the Mn_{0.15}Ce_{0.85} catalyst, reduction starts at 150 °C and the TPR profile consists of three overlapping peaks at 250, 350 and 420 °C. The TPR profile of the Mn_{0.25}Ce_{0.75} catalyst is similar to the one of Mn_{0.15}Ce_{0.85}, the only difference being that reduction starts at even lower temperature (~130 °C). Two reduction peaks at 270 and 380 °C are present in the profile of the Mn_{0.50}Ce_{0.50} catalyst, while one peak at 420 °C is present in the TPR profile of Mn_{0.75}Ce_{0.25} catalyst. The assignment of the

aforementioned peaks to different MnO_x species or to specific reduction steps is not straightforward, because reduction of ceria takes place concurrently. This can be easily deduced from the results presented in Table 3, which compare the amount of water produced during TPR to the theoretical ones corresponding to the reduction of Mn₃O₄, Mn₂O₃ or MnO₂ to MnO. It can be observed that for catalysts with Mn content up to 25 at.% the amount of produced water is significantly larger than the theoretical values, even if it is assumed that all manganese is present as Mn⁴⁺. This implies that reduction of Ce⁴⁺ to Ce³⁺ takes place along with reduction of manganese ions. The extent of CeO₂ reduction for each Mn–Ce catalyst is presented in Table 3 assuming that manganese in the catalysts is initially present either as Mn₂O₃ or Mn₃O₄. The calculations indicate that for catalysts with Mn content up to 25 at.% the extent of ceria reduction is of the order of 40–60%, i.e. approximately half of the Ce⁴⁺ ions present in the catalyst get reduced to Ce³⁺ ions. In the case of the Mn_{0.50}Ce_{0.50} and Mn_{0.75}Ce_{0.25} catalysts, the uncertainty in the estimation of the extent of ceria reduction is quite high because ceria content is lower and the exact average oxidation state of Mn ions is not known. XRD indicated the presence of a crystalline Mn₃O₄ phase in these catalysts, but the intensity of the relevant XRD peaks is rather low and the possibility of the coexistence of additional amorphous manganese oxide phases cannot be disregarded. Arena et al. [27] have reported on hydrogen consumption during TPR of Mn–Ce catalysts prepared by a new “redox-precipitation” route. Their results indicate that ceria reduction takes place along with

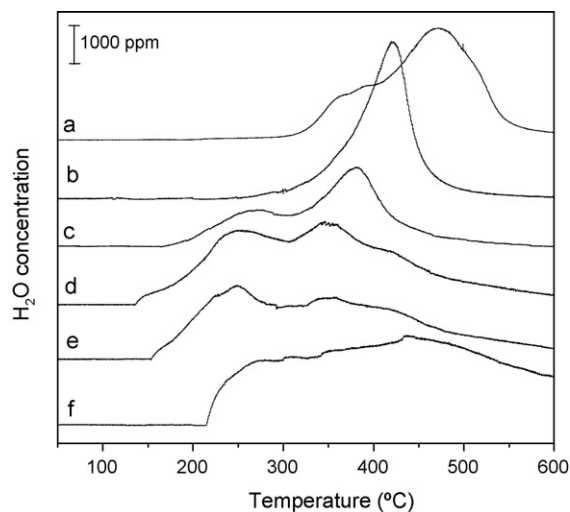


Fig. 4. TPR profiles of Mn–Ce catalysts. (a) MnO_x; (b) Mn_{0.75}Ce_{0.25}; (c) Mn_{0.5}Ce_{0.5}; (d) Mn_{0.25}Ce_{0.75}; (e) Mn_{0.15}Ce_{0.85}; (f) Mn_{0.05}Ce_{0.95}.

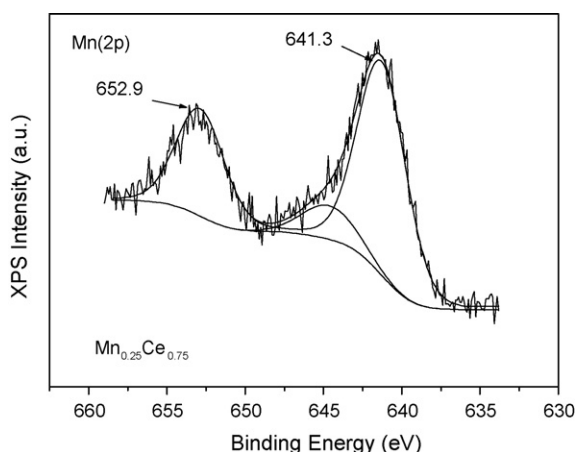


Fig. 5. Mn 2p XP spectrum of $\text{Mn}_{0.25}\text{Ce}_{0.75}$ catalyst.

reduction of manganese ions for the material with composition $\text{Mn}_{0.25}\text{Ce}_{0.75}$.

The oxidation state of catalyst surface species was examined by XPS analysis. The binding energies of the XPS $\text{Mn } 2p_{3/2}$ peaks in the $\text{Mn}_x\text{Ce}_{1-x}$ catalysts were found to be in the range 641.2–641.5 eV. An example of Mn 2p doublet analysis is depicted in Fig. 5. The spin orbit splitting is $\Delta E = 11.6$ eV and the width is 3.62 eV. The broadening at about 644.6 eV is attributed to Mn $2p_{3/2}$ energy losses. The binding energy of the Mn $2p_{3/2}$ component is at 641.3 eV. The aforementioned analysis leads to similar results for all catalysts. According to literature data [18] the observed binding energy corresponds to Mn_2O_3 . It should be noted, though, that the BEs of various Mn ions are very close to each other, rendering impossible the exact identification of oxidation states due to overlap of the energy ranges for various oxidation states of Mn [11,12]. However, the fact that the Mn $2p_{3/2}$ peak is rather broad may imply the co-existence of Mn^{2+} and Mn^{3+} ions at the surface of the catalysts. The XPS results do not provide any evidence for the presence of Mn^{4+} species (642.2–643 eV) [11,12]. The XPS O 1s spectra showed a main peak at a binding energy of 529.1–529.6 eV, corresponding to lattice oxygen of CeO_2 and MnO_x phases [18,28]. A broad shoulder at the higher binding energy region (531.5–532.7 eV) was evident in all samples and can be assigned to adsorbed hydroxyl groups [28]. The energy positions of the Ce 3d peaks correspond to Ce^{4+} in CeO_2 [28], suggesting that the presence of manganese ions does not affect the oxidation state of cerium.

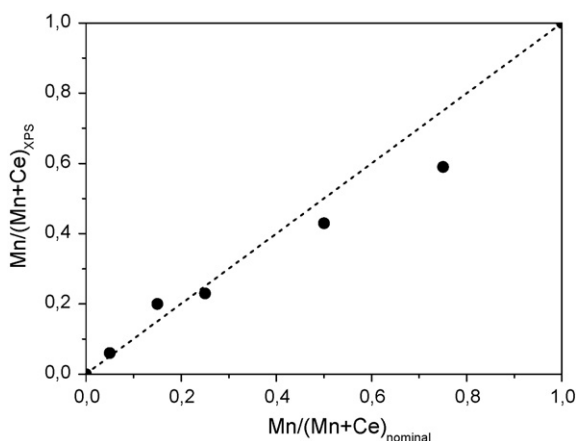


Fig. 6. XPS $\text{Mn}/(\text{Mn} + \text{Ce})$ atomic ratio vs. nominal atomic ratio.

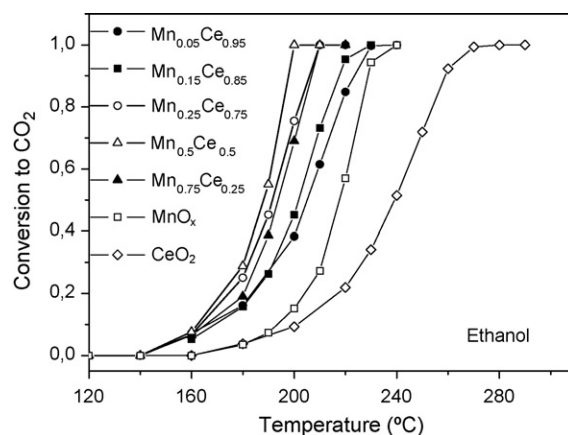


Fig. 7. Conversion of ethanol to CO_2 over Mn–Ce catalysts.

The surface composition of all catalysts, expressed as atomic $\text{Mn}/(\text{Mn} + \text{Ce})$ ratio, has been calculated from the intensity of the XPS Mn 2p and Ce 3d peaks using the atomic sensitivity factors of 2.6 and 10, respectively [29], and is compared to the corresponding nominal values in Fig. 6. It can be observed that the surface atomic $\text{Mn}/(\text{Mn} + \text{Ce})$ ratio is nearly equal to the nominal ratio for a Mn content up to 25 at.% indicating a homogeneous distribution of manganese ions in the bulk and the surface. Similar observations have been made by Machida et al. for binary Mn–Ce oxides prepared by co-precipitation [18]. With further increase in the manganese content to 50 and 75 at.%, the surface ratio becomes smaller than the nominal ratio, which is in agreement with the concomitant appearance of a crystalline Mn_3O_4 phase, as found by XRD.

3.3. Catalytic performance in VOC oxidation

The catalytic performance of MnO_x , CeO_2 and mixed $\text{Mn}_x\text{Ce}_{1-x}$ catalysts was evaluated in the oxidation of ethanol, ethyl acetate and toluene. The conversion of ethanol to CO_2 as a function of temperature is presented in Fig. 7. The least active catalyst is CeO_2 followed by MnO_x . Upon addition of MnO_x to ceria the activity increases monotonically up to a Mn content of 50 at.% and $\text{Mn}_{0.50}\text{Ce}_{0.50}$ is the most active among all catalysts achieving complete ethanol conversion to CO_2 at 200 °C. By comparison, the MnO_x catalyst achieves full conversion at 240 °C and CeO_2 at 280 °C. The corresponding results referring to ethyl acetate

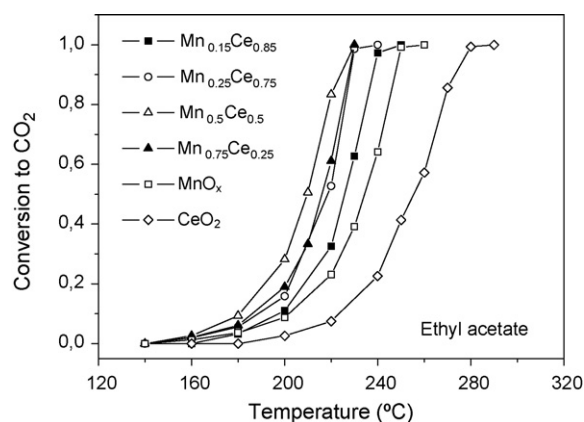


Fig. 8. Conversion of ethyl acetate to CO_2 over Mn–Ce catalysts.

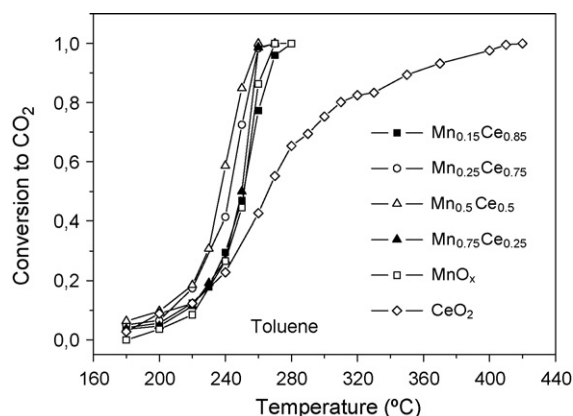


Fig. 9. Conversion of toluene to CO_2 over Mn–Ce catalysts.

oxidation are presented in Fig. 8. The catalyst ranking is identical to the one found in ethanol oxidation. All catalysts are less active in ethyl acetate oxidation and complete conversion to CO_2 takes place at temperatures higher by $\sim 20^\circ\text{C}$ compared to ethanol. In the case of toluene oxidation, the $\text{Mn}_{0.50}\text{Ce}_{0.50}$ sample is again the most active, although differences among the catalysts are less pronounced. The behaviour of CeO_2 in toluene oxidation should be noted: at low temperatures it has comparable activity to the other catalysts, but complete conversion of toluene requires temperatures higher than 400°C . Toluene is the most resistant to oxidation among the three VOCs examined and complete conversion is achieved at 260°C over the $\text{Mn}_{0.50}\text{Ce}_{0.50}$ catalyst (Fig. 9).

The single carbon-containing product of toluene oxidation was CO_2 at all conversion levels. On the other hand, acetaldehyde and small amounts of ethyl acetate were intermediate products during ethanol oxidation over all catalysts. Fig. 10 presents the conversion of ethanol to acetaldehyde, ethyl acetate and CO_2 over CeO_2 , $\text{Mn}_{0.50}\text{Ce}_{0.50}$ and MnO_x catalysts. Acetaldehyde is the major intermediate product in the course of ethanol oxidation towards CO_2 . Larger amounts of acetaldehyde are produced over MnO_x and Mn–Ce catalysts compared to CeO_2 . Actually, acetaldehyde is the single product of the reaction over MnO_x and $\text{Mn}_{0.50}\text{Ce}_{0.50}$ at low temperatures. Traces of ethyl acetate are also produced over all catalysts. The presence of ethyl acetate in the products indicates that acetate species are formed on the catalyst surface and they react with adsorbed ethanol via an esterification reaction. The

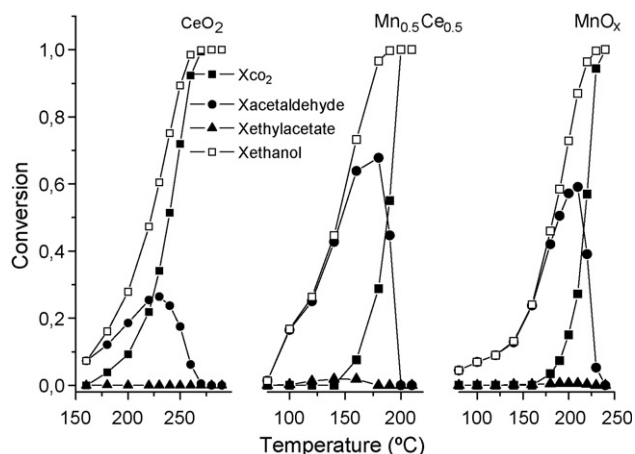


Fig. 10. Product distribution of ethanol oxidation over CeO_2 , $\text{Mn}_{0.5}\text{Ce}_{0.5}$ and MnO_x catalysts (Feed: 1600 ppm ethanol in air, $W/F = 0.072 \text{ g s cm}^{-3}$).

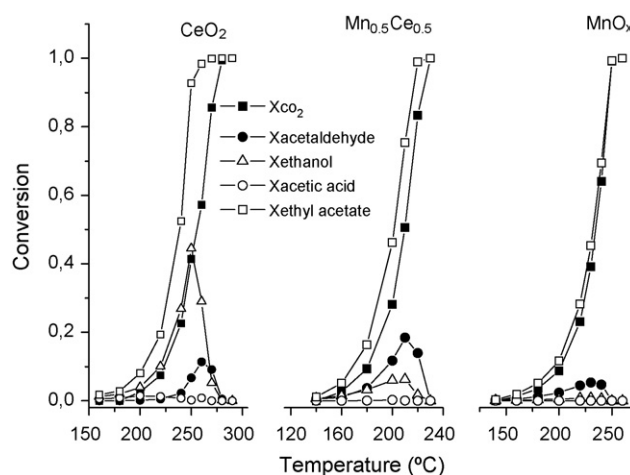
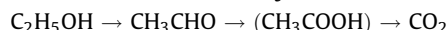


Fig. 11. Product distribution of ethyl acetate oxidation over CeO_2 , $\text{Mn}_{0.5}\text{Ce}_{0.5}$ and MnO_x catalysts (Feed: 1800 ppm ethyl acetate in air, $W/F = 0.072 \text{ g s cm}^{-3}$).

observed product distribution implies that total oxidation of ethanol over Mn–Ce catalysts is a series reaction:



The major path appears to be the direct oxidation of acetaldehyde to CO_2 , while its oxidation via the acetic acid should be a minor path, because no acetic acid is detected in the products and ethyl acetate production is minimal. Moreover, acetic acid is oxidized at higher temperatures than ethanol (as will be presented later on) and if it was produced in the course of ethanol oxidation, it should certainly appear in the reaction products.

In the case of ethyl acetate oxidation, acetaldehyde, ethanol, acetic acid and CO_2 were the carbon-containing products of the reaction. Fig. 12 depicts the conversion of ethyl acetate to these products over CeO_2 , $\text{Mn}_{0.50}\text{Ce}_{0.50}$ and MnO_x catalysts. The presence of ethanol and acetic acid as intermediate products indicates that the first step in ethyl acetate oxidation is its “hydrolysis” towards the corresponding alcohol and acid compounds, while the presence of acetaldehyde originates from partial oxidation of ethanol. The amount of acetic acid in the products is considerably lower than that of ethanol and acetaldehyde implying that acetic acid is oxidized at a faster rate than the other two molecules under the specific reaction conditions. In order to further study this point, we carried out the oxidation of acetic acid over the $\text{Mn}_{0.50}\text{Ce}_{0.50}$ catalyst and the results are presented in Fig. 12 along with those of

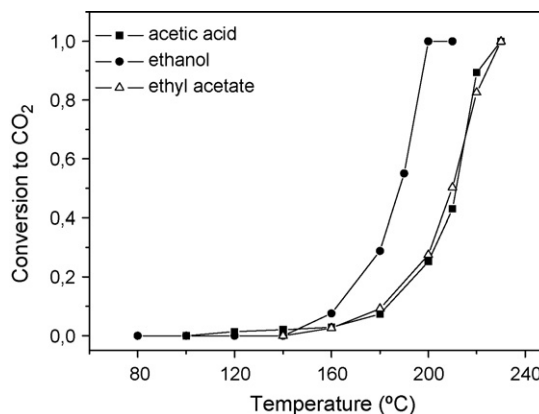


Fig. 12. Comparison of conversion of acetic acid, ethanol and ethyl acetate to CO_2 over the $\text{Mn}_{0.5}\text{Ce}_{0.5}$ catalyst.

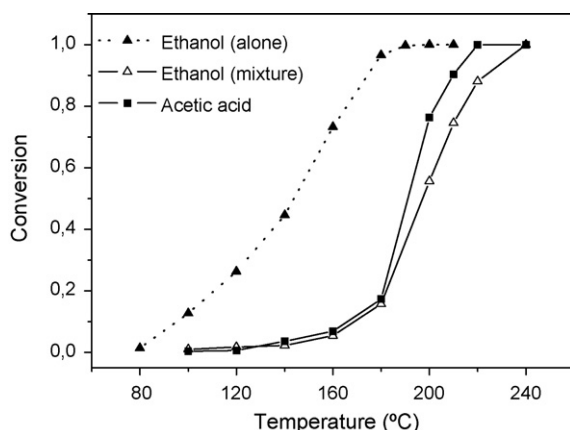


Fig. 13. Comparison of ethanol conversion when oxidized alone or in mixture with acetic acid (700 ppm ethanol + 600 ppm acetic acid in air) over the $\text{Mn}_{0.5}\text{Ce}_{0.5}$ catalyst.

ethanol and ethyl acetate oxidation for comparison. It can be observed that ethanol is the easiest to oxidize molecule, while the conversion curves of acetic acid and ethyl acetate are essentially identical. This result implies that acetic acid is inhibiting ethanol oxidation, as indeed observed in Fig. 13, which presents the conversion of ethanol in two cases: (i) when fed alone and (ii) when fed together with acetic acid. When acetic acid is present, the conversion of ethanol is completely suppressed and oxidation of ethanol follows the one of acetic acid. This behaviour can be explained by assuming that acetic acid is more strongly adsorbed than ethanol on Mn–Ce catalysts. The experiments described above indicate that the oxidation of ethyl acetate is determined by the reactivity of acetic acid (Fig. 12), which is produced as an intermediate, blocks the catalytic sites and drives off ethanol and acetaldehyde into the gas phase.

The performance of the most active $\text{Mn}_{0.50}\text{Ce}_{0.50}$ catalyst was also examined in the presence of CO_2 or H_2O in the VOC/air feed, as these compounds are commonly found in typical VOC-containing exhaust streams. Regarding the effect of CO_2 , it was found that addition of up to 20% CO_2 has a negligible effect on catalyst activity, without affecting measurably the temperature required for complete conversion of ethanol. The presence of 1.5% H_2O , on the other hand, has an inhibiting effect on VOC conversion to CO_2 over the $\text{Mn}_{0.5}\text{Ce}_{0.5}$ catalyst, as depicted in Fig. 14. In the case of ethanol, the temperature required for complete conversion to CO_2 is shifted by 10 °C to higher values. In the case of ethyl acetate, the

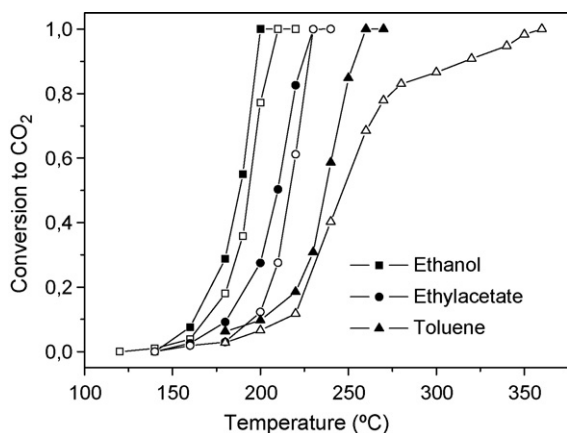


Fig. 14. Effect of H_2O added in feed on VOC oxidation over the $\text{Mn}_{0.5}\text{Ce}_{0.5}$ catalyst. Solid symbols: without H_2O , open symbols: with 1.5% H_2O in feed.

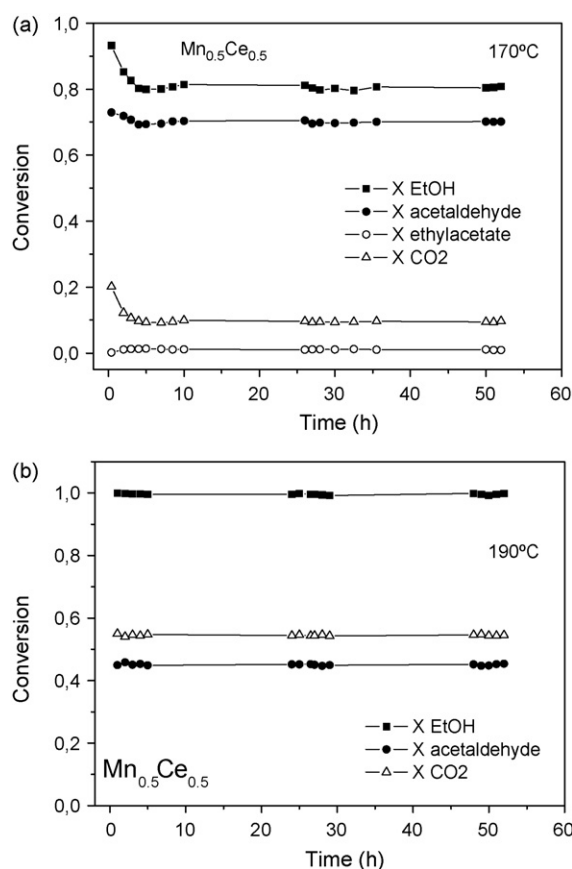


Fig. 15. Stability of $\text{Mn}_{0.5}\text{Ce}_{0.5}$ catalyst under ethanol oxidation conditions at: (a) 170 °C; (b) 190 °C.

temperature required for complete conversion to CO_2 is not shifted appreciably, although conversion to CO_2 is always smaller in the presence of water at lower temperatures. On the other hand, the presence of water enhances slightly the conversion of ethyl acetate to ethanol at low reaction temperatures (due to the hydrolysis reaction—not shown in Fig. 14). In the case of toluene oxidation, the effect of water is rather small at low reaction temperatures, but complete conversion of toluene to CO_2 is shifted considerably (by 100 °C) to higher temperatures.

The stability of the $\text{Mn}_{0.5}\text{Ce}_{0.5}$ catalyst under conditions of ethanol oxidation was assessed with experiments lasting over 50 h at 170 °C and 190 °C. These temperatures are lower than those required for complete conversion of ethanol to CO_2 and, thus, allow for facile detection of possible catalyst deactivation. The catalyst performance as a function of time-on-stream is presented in Fig. 15a and b for reaction temperatures of 170 and 190 °C, respectively. It can be observed that at 190 °C the $\text{Mn}_{0.5}\text{Ce}_{0.5}$ catalyst is perfectly stable over the period of 50 h. Ethanol is completely converted towards 45% acetaldehyde and 55% CO_2 . An initial transition period of 4–5 h is observed at 170 °C (Fig. 15a), during which the conversion of ethanol decreases from 95% to 82%, while ethyl acetate formation gradually increases from 0 to ~1%. The trends observed indicate that the decrease in ethanol conversion is due to build-up of adsorbed species on the catalyst surface until a steady-state is reached. Following this transition period, the catalyst is perfectly stable for the remaining duration of the test.

The activity of $\text{Mn}_x\text{Ce}_{1-x}$ catalysts in the oxidation of ethanol, ethyl acetate and toluene is higher than the one of pure MnO_x and CeO_2 oxides as shown in Figs. 7–9. The differential reaction rates on

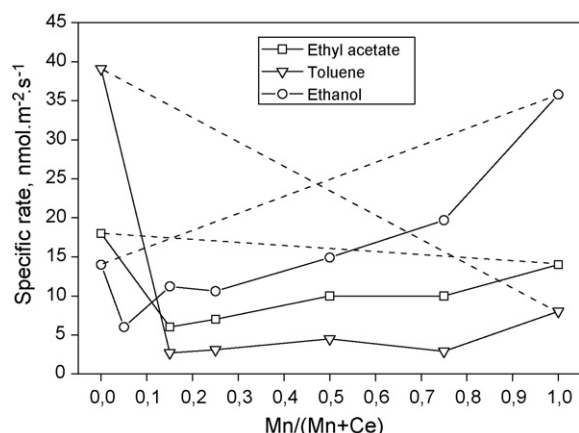


Fig. 16. Specific reaction rate of VOC oxidation as a function of Mn/(Mn + Ce) ratio.

a mass basis are generally 2–10 times higher over the $\text{Mn}_x\text{Ce}_{1-x}$ catalysts compared to the pure oxides. A more appropriate comparison among the various catalysts can be made, however, via the specific reaction rate per unit surface area. The specific reaction rate (in $\text{nmol m}^{-2} \text{s}^{-1}$) of all catalysts in the oxidation of ethanol, ethyl acetate and toluene is depicted in Fig. 16 as a function of the Mn/(Mn + Ce) atomic ratio. The dashed lines in the Figure correspond to the expected activity of a CeO_2 – MnO_x physical mixture. Due to the different reactivity of each VOC, the reaction rates have been calculated at different temperatures: 180 °C for ethanol and 200 °C for ethyl acetate and toluene. The specific activity of CeO_2 is higher than the one of MnO_x in ethyl acetate and toluene oxidation but lower in ethanol oxidation. Regarding toluene oxidation, all $\text{Mn}_x\text{Ce}_{1-x}$ catalysts have specific activities in the range 2.7–4.5 $\text{nmol m}^{-2} \text{s}^{-1}$ compared to 8 $\text{nmol m}^{-2} \text{s}^{-1}$ (MnO_x) and 39 $\text{nmol m}^{-2} \text{s}^{-1}$ (CeO_2). It should be noted that although CeO_2 appears to have the highest specific activity in toluene oxidation under differential conditions, it, nevertheless, achieves complete conversion of toluene at much higher temperatures than all other catalysts. In the case of ethanol oxidation, the specific activities of $\text{Mn}_x\text{Ce}_{1-x}$ catalysts increase with increase of Mn content from 6 to 19.7 $\text{nmol m}^{-2} \text{s}^{-1}$, while the specific activities of pure oxides are 14 $\text{nmol m}^{-2} \text{s}^{-1}$ (CeO_2) and 35.8 $\text{nmol m}^{-2} \text{s}^{-1}$ (MnO_x). In the case of ethyl acetate oxidation, the specific activities of $\text{Mn}_x\text{Ce}_{1-x}$ catalysts increase with increase of Mn content from 6 to 10 $\text{nmol m}^{-2} \text{s}^{-1}$, while the specific activities of pure oxides are 18 $\text{nmol m}^{-2} \text{s}^{-1}$ (CeO_2) and 14 $\text{nmol m}^{-2} \text{s}^{-1}$ (MnO_x). The specific surface areas of $\text{Mn}_x\text{Ce}_{1-x}$ catalysts, being considerably larger than the ones of pure oxides, overcompensate the decrease in specific activity. This is clearly evidenced in Figs. 7–9 presented in previous sections. The cause of the lower specific activity of Mn–Ce catalysts is not clear. XRD results (Fig. 2) showed that the pure manganese oxide catalyst is present in the Mn_2O_3 phase, while the Mn_3O_4 phase is detected in manganese-rich Mn–Ce catalysts. Testing of commercial Mn_2O_3 and Mn_3O_4 materials in EtOH oxidation showed that they have similar activities, with Mn_3O_4 being actually slightly more active than Mn_2O_3 . Therefore, the observed trend cannot be explained by the different oxidation state (and crystalline phase) of manganese oxide in Mn–Ce and pure MnO_x catalysts. The specific activity in ethanol oxidation of $\text{Mn}_{0.25}\text{Ce}_{0.75}$ catalysts synthesized with different urea equivalence ratios, Φ , has been also calculated. These catalysts have varying surface area values due to the effect of Φ variation. The calculations show that the specific activity increases with decrease of Φ . The catalyst prepared from the lowest equivalence ratio ($\Phi = 1.53$, Table 1) has the lowest surface area and, at the same time, the highest specific activity

(67 $\text{nmol m}^{-2} \text{s}^{-1}$), while the activity of the reference $\text{Mn}_{0.25}\text{Ce}_{0.75}$ catalyst prepared from $\Phi = 5.20$ is 11 $\text{nmol m}^{-2} \text{s}^{-1}$. By comparison, the activities of pure CeO_2 and MnO_x are 14 and 36 $\text{nmol m}^{-2} \text{s}^{-1}$, respectively.

Benchmarking of the catalytic performance of $\text{Mn}_x\text{Ce}_{1-x}$ catalysts studied in this work with respect to other Mn-based catalysts presented in the literature is not an easy task because of the varying experimental conditions. Refs. [4–6] report on the ethanol oxidation activity of MnO_x catalysts prepared by oxidative decomposition of MnCO_3 and oxidation of acidic MnSO_4 solution. Total conversion of ethanol was obtained at ~ 180 °C at a W/F ratio of 0.6 g s cm^{-3} . Peluso et al. [7] examined ethanol oxidation over MnO_x catalysts prepared by reaction of $\text{Mn}(\text{NO}_3)_2$ with KMnO_4 . Total conversion of ethanol was obtained at ~ 170 °C at a W/F ratio of 0.6 g s cm^{-3} . The MnO_x sample of the present work achieved complete ethanol conversion at 240 °C at a W/F ratio of 0.072 g s cm^{-3} , i.e. at an almost an order of magnitude higher space velocity. Rao et al. [12] examined ethanol oxidation over a $\text{Mn}_{0.10}\text{Ce}_{0.90}$ catalyst prepared by a citric-acid sol–gel method. The temperature at 50% yield of CO_2 (T_{50}) from a 1.5% ethanol feed was 250 °C at a space velocity of 30,000 h^{-1} . $\text{Mn}_{0.05}\text{Ce}_{0.95}$ and $\text{Mn}_{0.15}\text{Ce}_{0.85}$ catalysts of the present work achieved 50% yield of CO_2 at 205–210 °C at a space velocity of 50,000 h^{-1} from a 0.16% ethanol feed. Ethyl acetate oxidation has been studied over a manganese oxide OMS-2 catalyst [8]. Complete conversion of ethyl acetate to CO_2 was observed at 400 °C with a space velocity of 20,000 h^{-1} , i.e. at temperatures significantly higher than those of the present work. Regarding toluene oxidation, a Mg/Mn/Al mixed oxide catalyst (14 at.% Mn) was found to achieve complete conversion of toluene at 360 °C at a space velocity of 30,000 h^{-1} [11]. Combustion-synthesized Mn–Ce catalysts appear to be superior than Mg/Mn/Al catalysts, as they achieve complete toluene conversion at 260 °C (SV = 50,000 h^{-1}). The activity of Mn–Ce catalysts of the present work competes quite favourably with the one of supported Pt catalysts. We have previously reported on the activity of Pt/ Al_2O_3 catalysts in ethanol oxidation. A 0.3 wt.% Pt/ Al_2O_3 catalyst achieves complete ethanol conversion at 270 °C at a W/F ratio of 0.072 g s cm^{-3} [30]. Promotion with potassium enhances platinum activity lowering the above temperature to 220 °C. Ethyl acetate oxidation over a 0.3 wt.% Pt/ Al_2O_3 catalyst requires temperatures above 300 °C. Pt catalysts supported on W-doped TiO_2 are considerably more active than Pt/ Al_2O_3 achieving complete mineralization of ethyl acetate at 240 °C [31].

The apparent activation energies, E_{app} , of CO_2 formation during ethanol, ethyl acetate and toluene oxidation over $\text{Mn}_x\text{Ce}_{1-x}$ catalysts are presented in Table 4. Apparent activation energies and prefactors were calculated from Arrhenius plots using the rate of CO_2 production expressed on a unit surface area basis ($\text{mol m}^{-2} \text{s}^{-1}$). The temperature range chosen for each catalyst was the one corresponding to low conversion to CO_2 (less than 20%). Overall, E_{app} values lie between 65 kJ mol^{-1} (toluene– CeO_2) and 126 kJ mol^{-1} (ethanol– MnO_x). The apparent activation energies measured over $\text{Mn}_x\text{Ce}_{1-x}$ catalysts get, generally, intermediate values in the range defined by the values measured over the CeO_2

Table 4
Apparent activation energies (kJ mol^{-1}) of VOC oxidation

Catalyst	Ethanol	Ethyl acetate	Toluene
CeO_2	85 ± 6	111 ± 7	65 ± 12
$\text{Mn}_{0.05}\text{Ce}_{0.95}$	82 ± 5	nm	nm
$\text{Mn}_{0.15}\text{Ce}_{0.85}$	98 ± 12	119 ± 4	93 ± 12
$\text{Mn}_{0.25}\text{Ce}_{0.75}$	113 ± 13	111 ± 10	100 ± 11
$\text{Mn}_{0.5}\text{Ce}_{0.5}$	114 ± 11	103 ± 3	77 ± 14
$\text{Mn}_{0.75}\text{Ce}_{0.25}$	105 ± 15	97 ± 13	106 ± 14
MnO_x	126 ± 6	95 ± 6	115 ± 10

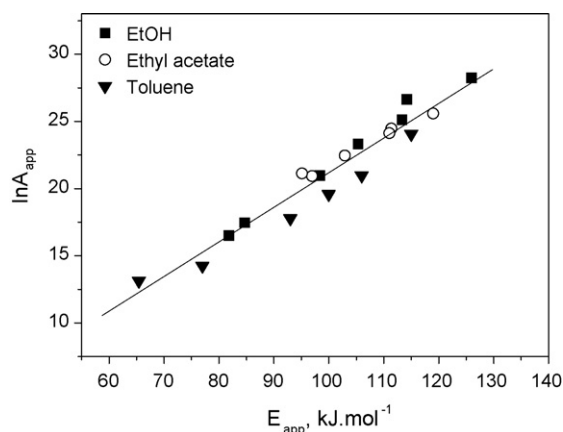


Fig. 17. Constable plot of apparent prefactors as a function of apparent activation energies for oxidation of ethanol, ethyl acetate and toluene over $\text{Mn}_x\text{Ce}_{1-x}$ catalysts.

and MnO_x catalysts. The Constable plot of apparent prefactors, $\ln A_{\text{app}}$, and apparent activation energies, E_{app} , of the reactions of ethanol, ethyl acetate and toluene oxidation over $\text{Mn}_x\text{Ce}_{1-x}$ catalysts is presented in Fig. 17. It can be observed that the data fit into the Cremer-Constable relation:

$$\ln A_{\text{app}} = aE_{\text{app}} + b \quad (7)$$

i.e., a compensation effect is present. The slope a of the straight line calculated by linear regression is 0.26 mol kJ^{-1} . Lyngaard et al. [32] have presented an elegant analysis, in which they show that the slope of the Constable plot should be equal to $\sim(RT)^{-1}$, where T is an average temperature of reaction rate measurements. In the present work, measurements were carried out in the temperature range of 140–220 °C. Assuming an average temperature of 180 °C, the $(RT)^{-1}$ term is $0.266 \text{ mol kJ}^{-1}$, which is in perfect agreement with the experimentally determined slope a . According to Lyngaard et al. [32], the compensation effect is observed for reactions showing nonlinearity in the Arrhenius plot. When specific reactions are compared over different catalysts, the nonlinearity is caused by differences in binding energies and activation enthalpies, which means that a compensation effect should be quite general, since these contributions are likely to vary. In both cases, the analysis of Lyngaard et al. shows that the slope in the Constable plot will be close to $(RT)^{-1}$, which means that it is independent of reaction mechanism and kinetics.

3.4. Overview

The observation that the specific activity of $\text{Mn}_x\text{Ce}_{1-x}$ catalysts prepared with ratio $\Phi = 5.2$ is lower than the one of pure CeO_2 and MnO_x is certainly noteworthy. On the other hand, the $\text{Mn}_{0.25}\text{Ce}_{0.75}$ catalyst prepared with ratio $\Phi = 1.53$, i.e. under conditions which favour sintering and the resulting surface area of the material is small, has a higher specific activity than CeO_2 or MnO_x in ethanol oxidation. Tang et al. [13] have examined the effect of calcination temperature on the activity of a $\text{Mn}_{0.50}\text{Ce}_{0.50}$ catalyst in formaldehyde oxidation. They found that the surface area of the catalyst decreases monotonically from 200 to $\sim 15 \text{ m}^2 \text{ g}^{-1}$, when the calcination temperature is increased from 300 to 700 °C. The activity, on the other hand, expressed as HCHO conversion shows a slight maximum for the catalyst calcined at 500 °C. The authors attribute the decrease in activity for catalysts calcined above 500 °C to segregation of MnO_x from the $\text{MnO}_x\text{--CeO}_2$ solid solution. However, if one calculates the specific activity per unit surface area of the catalysts, it turns out that it increases continuously with

increase of calcination temperature and concomitant decrease of surface area. If the specific activity is expressed as $(\% \text{HCHO Conversion m}^{-2})$, it is 0.115 m^{-2} for $T_{\text{calc}} = 300 \text{ °C}$ and 1 m^{-2} for $T_{\text{calc}} = 700 \text{ °C}$. Chen et al. [15] have investigated the wet oxidation of phenol over Mn--Ce catalysts with varying atomic ratio. In this specific reaction CeO_2 is inactive and MnO_x is active. The specific activity of Mn--Ce catalysts was observed to decrease with increase of Ce content and all Mn--Ce catalysts show lower specific activity than pure MnO_x . The results of the aforementioned studies are in line with our observations.

Characterization of combustion-prepared Mn--Ce catalysts has shown that the presence of both ions inhibits crystallite growth during synthesis resulting in mixed oxides with higher surface area than pure oxide counterparts. This effect is not specific to the combustion method, as it has been also observed for Mn--Ce catalysts prepared by co-precipitation [15]. XRD and XPS measurements have provided evidence of incorporation of Mn ions in the ceria fluorite structure at low Mn loadings. At high Mn loadings, segregation of a Mn_3O_4 phase takes place. The presence of ceria influences the oxidation state of manganese, because pure MnO_x crystallizes in the Mn_2O_3 phase. The reducibility of Mn--Ce catalysts is significantly enhanced compared to the pure oxides, as found using hydrogen as reducing agent, indicating the presence of more labile oxygen species in these materials. Similar observations have been made by other investigators for Mn--Ce catalysts prepared by co-precipitation and combustion methods [13,14,24]. A new finding of the present work, is that extensive reduction of ceria takes place alongside MnO_x reduction. This is analogous to what has been found during reduction of CuO--CeO_2 catalysts [33]. It is interesting that the enhancement of reducibility upon combination of Mn and Ce oxides – as inferred by H_2 -TPR results – is not translated into a higher specific activity in VOC oxidation. This may be attributed to the fact that the reducing agent under reaction conditions is of course the VOC molecule and not H_2 as in TPR. The changes induced in reducibility (as probed by H_2) upon combination of Mn and Ce oxides probably do not apply when VOCs are the reducing agents instead of H_2 . An additional contributing factor could be that, in contrast to H_2 , VOC molecules get adsorbed on the catalyst surface under reaction conditions. The absence of correlation between catalyst reducibility by H_2 and activity in VOC oxidation certainly deserves further attention and dynamic experiments of ethanol adsorption and surface reaction are currently in progress to gain insight on the origin of this behaviour.

The course of ethanol oxidation over Mn--Ce catalysts is clearly indicative of a series reaction scheme, i.e. ethanol gets oxidized to acetaldehyde and acetaldehyde gets oxidized to CO_2 . The contribution of a step comprising acetaldehyde oxidation via intermediate formation of acetic acid is minor, as deduced from: (i) the absence of acetic acid in the products and (ii) the presence of traces of ethyl acetate in the products, which shows that the amount of acetate species formed on the catalyst surface must be small. If acetic acid formation was a major path, then ethanol and acetic acid should get oxidized at comparable rates, which is not the case (Fig. 12). The series reaction scheme appears to be valid for several Mn-containing catalysts [5,9,34]. Ethanol oxidation over $\text{Pt/Al}_2\text{O}_3$ catalysts, on the other hand, proceeds through intermediate formation of both acetaldehyde and acetic acid [30]. The yield of CH_3CHO is higher over MnO_x and Mn-rich catalysts than over CeO_2 or Ce-rich catalysts. Trawczynski et al. [9] have attributed the high yield of acetaldehyde over MnO_x to the absence of acidic sites on its surface. The activity of MnO_x catalysts in ethanol oxidation has been often correlated to the presence of both Mn^{4+} and Mn^{3+} ions, as well as of Mn^{4+} vacancies [5,6]. Mn^{4+} ions do not seem, however, to be a prerequisite for high activity.

Mn–Ce catalysts of the present work exhibit high activity, although they contain no Mn^{4+} ions. A MnO_x/YSZ catalyst, whose characterization did not provide indications of the presence of Mn^{4+} , has been also reported to be highly active in ethanol oxidation [9].

Oxidation of ethyl acetate proceeds via dissociation of the parent molecule to ethanol and acetic acid. Ethanol gets oxidized to CO_2 via acetaldehyde and the relative amounts of ethanol and acetaldehyde are determined by the behaviour of the catalyst in ethanol oxidation itself (Figs. 10 and 11). Acetic acid is preferentially oxidized due to its stronger binding on the surface compared to ethanol and the rate determining step of ethyl acetate oxidation is the oxidation of acetic acid formed as intermediate product. Ethanol and acetaldehyde were also found to be intermediate products during ethyl acetate oxidation over $\text{La}_{0.8}\text{Sr}_{0.2}\text{MnO}_{3+x}$ perovskites [34]. Oxidation of ethyl acetate over supported Pt catalysts, on the other hand, leads to formation of acetic acid as intermediate product [31].

The temperatures required for complete conversion of ethanol, ethyl acetate and toluene to CO_2 were the lowest over the $\text{Mn}_{0.50}\text{Ce}_{0.50}$ catalyst. This is in line with results of Chen et al. [15], who found that the highest conversion of phenol under wet oxidation conditions is obtained over catalysts with a Mn/Ce ratio around unity. Likewise, the lowest T_{50} and T_{95} temperatures of hexane oxidation were observed over a $\text{Mn}_{0.50}\text{Ce}_{0.50}$ catalyst [14].

4. Conclusions

The properties of $\text{MnO}_x\text{--CeO}_2$ catalysts prepared by a combustion method depend on the Mn/(Mn + Ce) atomic ratio. At Mn/(Mn + Ce) ratios up to 0.25, a major fraction of Mn ions are incorporated in the ceria lattice and a homogeneous distribution of Mn ions in the bulk and the surface of the catalysts is evident. At Mn/(Mn + Ce) ratios higher than 0.25, segregation of a separate Mn_3O_4 phase takes place. Both Mn^{2+} and Mn^{3+} ions appear to be present on the surface of the catalysts. Reduction of $\text{MnO}_x\text{--CeO}_2$ materials by hydrogen takes place at lower temperatures than those of pure MnO_x and the presence of Mn ions induces extensive reduction of Ce^{4+} ions. Interaction between MnO_x and CeO_2 leads to structural and thermal stabilization of the catalysts and their specific surface areas are greater than the ones of pure MnO_x or CeO_2 . The specific activity of $\text{MnO}_x\text{--CeO}_2$ catalysts in the oxidation of ethanol, ethyl acetate and toluene is lower than the one of pure MnO_x and CeO_2 , but, in practice, mixed oxide catalysts achieve

complete VOC conversion to CO_2 at lower temperatures due to their larger surface area. $\text{MnO}_x\text{--CeO}_2$ catalysts with high specific activity can be synthesized at low urea equivalence ratios, but under these conditions the surface area of the final material is low. A compensation effect is present during oxidation of the three studied VOCs over the catalysts of this work.

References

- [1] P. Papaefthimiou, T. Ioannides, X.E. Verykios, *Appl. Catal. B* 15 (1998) 75.
- [2] K. Okumura, T. Kobayashi, H. Tanaka, M. Niwa, *Appl. Catal. B* 44 (2003) 325.
- [3] C. Lahousse, A. Bernier, P. Grange, B. Delmon, P. Papaefthimiou, T. Ioannides, X. Verykios, *J. Catal.* 178 (1998) 214.
- [4] M.A. Peluso, J.E. Sambeth, H.J. Thomas, *React. Kinet. Catal. Lett.* 80 (2003) 241.
- [5] L. Lamaita, M.A. Peluso, J.E. Sambeth, H.J. Thomas, *Appl. Catal. B* 61 (2005) 128.
- [6] L. Lamaita, M.A. Peluso, J.E. Sambeth, H.J. Thomas, G. Minelli, P. Porta, *Catal. Today* 107–108 (2005) 133.
- [7] M.A. Peluso, E. Pronisato, J.E. Sambeth, H.J. Thomas, G. Busca, *Appl. Catal. B* 78 (2008) 73.
- [8] A.R. Gandhe, J.S. Rebello, J.L. Figueiredo, J.B. Fernandes, *Appl. Catal. B* 72 (2007) 129.
- [9] J. Trawczynski, B. Bielak, W. Mista, *Appl. Catal. B* 55 (2005) 277.
- [10] P.-O. Larsson, A. Andersson, *Appl. Catal. B* 24 (2000) 175.
- [11] R. Dula, R. Janik, T. Machej, J. Stoch, R. Grabowski, E.M. Serwicka, *Catal. Today* 119 (2007) 327.
- [12] T. Rao, M. Shen, L. Jia, J. Hao, J. Wang, *Catal. Comm.* 8 (2007) 1743.
- [13] X. Tang, Y. Li, X. Huang, Y. Xu, H. Zhu, J. Wang, W. Shen, *Appl. Catal. B* 62 (2006) 265.
- [14] G. Picasso, M. Gutierrez, M.P. Pina, J. Herguido, *Chem. Eng. J.* 126 (2007) 119.
- [15] H. Chen, A. Sayari, A. Adnot, F. Larachi, *Appl. Catal. B* 32 (2001) 195.
- [16] A.M.T. Silva, R.R.N. Marques, R.M. Quinta-Ferreira, *Appl. Catal. B* 47 (2004) 269.
- [17] G. Qi, R.T. Yang, R. Chang, *Appl. Catal. B* 51 (2004) 93.
- [18] M. Machida, M. Uto, D. Kurogi, T. Kijima, *Chem. Mater.* 12 (2000) 3158.
- [19] G. Avgouropoulos, T. Ioannides, *Appl. Catal. A* 244 (2003) 155.
- [20] J. Papavasiliou, G. Avgouropoulos, T. Ioannides, *Catal. Comm.* 6 (2005) 497.
- [21] D.A.M. Monti, A. Baiker, *J. Catal.* 83 (1983) 323.
- [22] P. Malet, A. Caballero, *J. Chem. Soc. Faraday Trans.* 84 (1988) 2369.
- [23] G. Avgouropoulos, T. Ioannides, *Appl. Catal. B* 67 (2006) 1.
- [24] B. Murugan, A.V. Ramaswamy, D. Srinivas, C.S. Gopinath, V. Ramaswamy, *Chem. Mater.* 17 (2005) 3983.
- [25] C.H.Y. Kang, H. Kusaba, H. Yahiro, K. Sasaki, Y. Teraoka, *Solid State Ionics* 177 (2006) 1799.
- [26] J. Carno, M. Ferrandon, E. Bjornbom, S. Jaras, *Appl. Catal. A* 155 (1997) 265.
- [27] F. Arena, G. Trunfio, J. Negro, B. Fazio, L. Spadaro, *Chem. Mater.* 19 (2007) 2269.
- [28] F. Larachi, J. Pierre, A. Adnot, A. Bernis, *Appl. Surf. Sci.* 195 (2002) 236.
- [29] D. Briggs, M.P. Seah, second ed., *Practical Surface Analysis*, vol. 1, Wiley, New York, 1996.
- [30] G. Avgouropoulos, E. Oikonomopoulos, D. Kanistras, T. Ioannides, *Appl. Catal. B* 65 (2006) 62.
- [31] P. Papaefthimiou, T. Ioannides, X.E. Verykios, *Appl. Therm. Eng.* 18 (1998) 1005.
- [32] H. Lynggaard, A. Andreassen, C. Stegelmann, P. Stoltze, *Prog. Surf. Sci.* 77 (2004) 71.
- [33] A. Pintar, J. Batista, S. Hocevar, *J. Colloid Int. Sci.* 285 (2005) 218.
- [34] V. Blasin-Aubé, J. Belkouch, L. Monceaux, *Appl. Catal. B* 43 (2003) 175.